35p

LTV RESEARCH CENTER

ABSTRACT

r 9298

A sensitive balance for making direct measurements of skin friction drag forces in the LTV Research Center boundary layer channel has been built and calibrated. The balance is a null-type instrument employing a crossed current and magnetic field to obtain a restoring force that balances the drag force. For a constant magnetic field the current required to null the balance is a linear function of the applied force resulting in a calibration factor of 0.220 milliamps per milligram of force. The balance will be used to measure wall shearing stress over a range of values up to 7.0 dynes/cm^2 (10^{-4} lb/in^2) with expected average accuracy of ± 1% for turbulent boundary layer flow.

The text of this report covers in detail the development and testing of a protytype model balance and the final design, calibration, and performance of the operational skin friction balance. Experimental data are presented to illustrate the quality of measurements that can be made with this instrument.

Arthur

TABLE OF CONTENTS

INTRODUCTION

Since the early years of the 20th century when the boundary layer concept was first introduced into the field of fluid mechanics there has been an ever increasing interest in the phenomenon of viscous or frictional drag. As the performance of modern day aircraft and naval vessels is constantly being extended, more and more attention is being focused on the problem of understanding the nature of viscous drag with the hope of being able to find methods by which its detrimental effects can be reduced. The speeds of vehicles operating in viscous media are now great enough that skin friction drag can account for a considerable portion of the total drag force, as much as 50 percent in some cases. It is therefore evident that effective methods for reducing skin friction drag forces are necessary in order to achieve optimization of future vehicle designs. These methods must come from a new and extended understanding of the boundary layer problem.

In 1960, the first steps were taken to establish a facility within the LTV Research Center for use in a program of experimental boundary layer research. It was felt that the highly non-linear nature of certain boundary layer flows required an intensive experimental investigation in order to obtain a detailed description of the various phenomena that occur. These experimental results would then serve as a foundation upon which new theories might be built. The facility that grew from these plans is the LTV Research Center boundary layer channel. A sketch of the facility is shown in Figure 1 and a complete description can be found in reference 1. Basically, the boundary layer channel is a straight plexiglass tube having a test section 25-feet long with an 8-inch internal diameter. The operating range of free stream velocities is from zero to approximately 55 feet per second.

The boundary layer channel was designed specifically for use in studies of the transition process from laminar to turbulent flow in the boundary layer, and experience has proved its ability to simulate the two-dimensional flat plate problem for laminar flow. The channel can also be used to produce turbulent boundary layer flow by artificially tripping the boundary layer. For this case the flow does not exactly duplicate that of the flat plate due to pressure gradient and three dimensional effects and analyses must be restricted to evaluations based on local flow conditions.

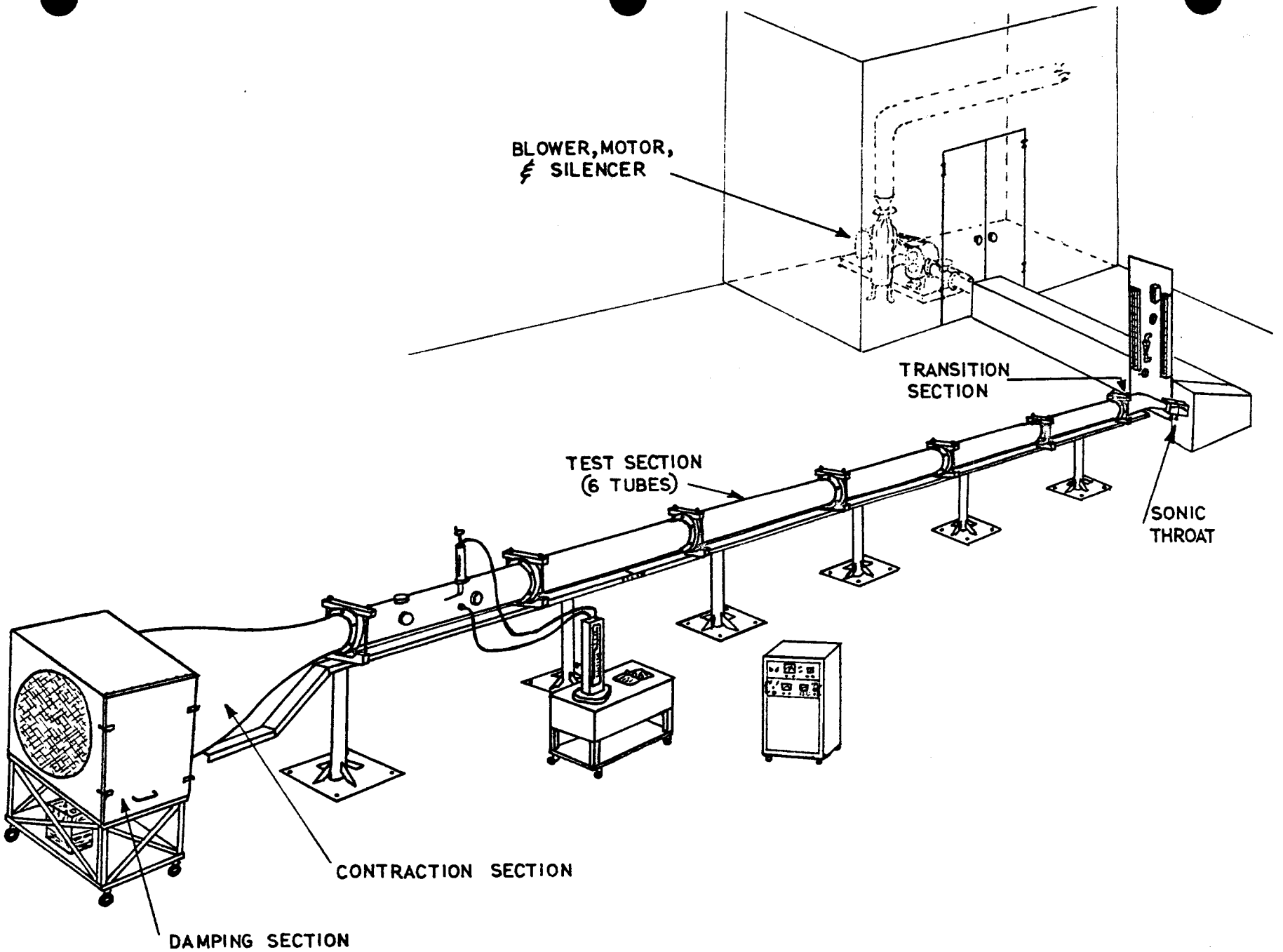

FIGURE 1. A PORTION OF THE AEROPHYSICS LABORATORY
SHOWING THE BOUNDARY LAYER CHANNEL

At the present time the boundary layer channel is being used in a study of turbulent boundary layer flow. The objective of the study is to determine the effects on a turbulent boundary layer caused by placing discrete disturbance producing elements on the bounding wall. Specific interest lies in the effect of the disturbance elements on skin friction drag and heat transfer with a more fundamental interest in gaining a detailed description of the basic flow phenomena under such conditions.

The purpose of this report is to describe an instrument that has been developed for use in the boundary layer channel in conjunction with the aforementioned experimental study of turbulent boundary layers.

INITIAL STUDIES

At the outset of the program to study the effects of discrete disturbance producing elements on fully developed turbulent boundary layers it was apparent that one requirement would be an accurate method of determining wall shearing stress. This is necessary to provide a basis for comparison of the effectiveness of the various disturbance producing elements.

Wall shearing stress can be determined by several methods for turbulent boundary layers. It can be related to the momentum deficit in the boundary layer as determined from velocity profile measurements provided that the pressure gradient is zero or that its effects can be accurately taken into account, it can be obtained with the aid of Newton's viscosity law and velocity measurements in the viscous sublayer, or it can be determined directly by measuring the friction drag force on a known segment of surface area. The last method employs an instrument commonly known as a skin friction balance for measuring the drag forces, and has been used with good success by several investigators. The first significant measurements of this type were made by Kempf (reference 2) and Schultz-Grunow (reference 3), and in more recent years many advancements in the technique have been made, notably by Coles (reference 4), Dhawan (reference 5), and Fenter (reference 6).

The first two methods mentioned above require that the velocity throughout the boundary layer be measured accurately. This is not easily done for a turbulent boundary layer, especially if the velocity profile is distorted and irregular as might be expected in the vicinity of any strong disturbance. The third method is not limited in this manner and was chosen as being the most promising due to its inherent independence of the nature of the boundary layer flow.

After the decision was made to use a skin friction balance as the primary instrument for obtaining wall shearing stress the first task was to determine its required specifications. To begin, the approximate range of wall shearing stress that would be encountered in the experiments had to be established. This was done by measuring a set of time averaged velocity profiles in a turbulent boundary layer flow on the smooth wall of the boundary layer channel for several flow rates and at several stations along the length of the channel.

The measurements were made with a constant-current hot wire anemometer and covered a range of Reynolds numbers from 3.3×10^3 to 1.2×10^4 based on the momentum thickness of the boundary layer. To allow for the effects of the moderate pressure gradient the wall shearing stress was calculated from the von Kármán momentum theorem (reference 7) in the form

$$\tau_o = \rho U_\infty^2 \left[\frac{d\theta}{dx} + (H + 2) \frac{\theta}{U_\infty} \frac{d U_\infty}{dx} \right] , \qquad (1)$$

where τ_o = wall shearing stress

ρ = fluid density

U_∞ = local mean velocity at outer edge of the boundary layer

θ = boundary layer momentum thickness defined as

$$\theta = \int_o^\infty \frac{u}{U_\infty} \left(1 - \frac{u}{U_\infty}\right) dy$$

u = local mean velocity in the boundary layer

x = distance parallel to the flow direction measured from an arbitrary origin

y = distance from the wall

H = boundary layer velocity profile shape parameter defined as $\frac{\delta^*}{\theta}$ where θ is as defined above and $\delta^* = \int_o^\infty \left(1 - \frac{u}{U_\infty}\right) dy$.

All of the parameters in the momentum equation were obtained from the velocity profiles and the calculations placed the maximum wall shearing stress for the undisturbed turbulent boundary layer in a range from 3.5 dynes/cm^2 (5×10^{-5} lb/in^2) to 7.0 dynes/cm^2 (10^{-4} lb/in^2).

A skin friction balance measures forces and the magnitude of the forces depends not only on the shear stress but also on the size of the surface element used with the balance. It is normally desirable to keep the surface element small so that a true local measurement can be made, but in this case a very small element would produce extremely small forces because of the low shear stresses. A disk 1.25 inches in diameter was chosen for the surface element which, for the calculated range of shear stress, will give a drag

force range from 6.0×10^{-5} lb. to 1.2×10^{-4} lb. It was believed that forces in this range can be measured with an accuracy on the order of 1 percent but the accuracy in measurements of smaller forces will probably decrease.

With the size of the surface element established, a survey was made of the balance methods used by previous investigators for drag force measurements. The most popular method seems to be one in which the surface element is supported by a flexure system that allows a small translation of the floating surface element when acted upon by the surface shearing stress. The displacement of the floating element is then calibrated as a function of the drag force and read by some type of accurate position indicator. Dhawan (reference 5) used this type of instrument with good success noting that the main sources of trouble were in keeping the surface of the floating element parallel with and recessed from the surrounding surface throughout its translation, and determining and correcting for the effect of pressure gradients in the flow direction as the gap between the floating element and surrounding surface changed geometry during translation of the element. Coles (reference 4) also used the same basic balance with the addition of a null feature whereby the element was mechanically returned to the same position for each measurement. The distance the element had to be moved from its initial displacement to the null position was measured with a micrometer and related to the drag force. A slightly different approach was tried by Smith and Walker (reference 8) at Ames Research Center. Their balance, which also operated on a null principle, had an element that was repositioned in the center of its cavity as each measurement was made by a variable strength electromagnet that provided the force necessary to counteract the drag force and null the balance.

Considering the nature of the boundary layer channel the null type balance was chosen as being the best suited. The curved wall could further complicate the problem of maintaining alignment and parallelism for a translating floating element, and the significant pressure gradient existing in the channel with turbulent boundary layer flow could be troublesome. The null type balance would minimize these problems by assuring the same geometry for the system during all measurements regardless of the magnitude of the drag force. The flexure system could also be simplified to be a simple pivot instead of the

four-bar type linkage necessary when the floating element is maintained parallel to its surroundings during movement.

At this point a detailed analysis was made to check the feasibility of using a null-type balance and to establish the necessary components.

A. Position Indicator

The heart of any null-type device is the component that indicates a nulled condition. In this case that component must monitor the position of the floating surface element of the balance. From previous personal experience and also from numerous references a differential transformer was known to be an excellent device for this purpose. One of the model 005MS-L linear variable differential transformers manufactured by the Schaevitz Engineering Co., Camden, New Jersey, was chosen. Some comments on the use of this transformer will be made later, but suffice it to say here that this model transformer, when excited with 5 volts at a frequency of 20 kilocycles per second, has an output signal change of 21.7 millivolts per 0.001 inch displacement of the core. Conservatively assuming a resolution of 0.5 millivolts in the output signal, changes in the position of the transformer core as small as 0.000023 inches can be measured.

B. Flexure System

As mentioned previously a null-type balance can have a simple pivot arrangement as the support flexure. The floating element can be fixed to one end of a beam which pivots within a fixed framework. The only restriction is that the pivot must be free of friction. This rules out the use of simple bearing type pivots. No matter how good a conventional bearing assembly is it will always have some amount of friction which cannot be accurately determined, and it was felt that for the measurement of the very small drag forces no friction at all could be tolerated because of the uncertainty it would put into the measurements.

The problem of frictionless bearings has been dealt with thoroughly by Eastman (reference 9). His paper describes a flexure system that acts as a true frictionless pivot through a restricted angle of rotation, having very small spring constants but capable of supporting appreciable loads. The only

friction involved is the molecular friction generated by the flexing of the members and this is quite negligible. A brief search revealed that the same type of pivot is now available commercially from the Bendix Corporation, Utica, New York, under the trade name of Bendix Free-flex Flexural Pivot.

In order to choose a particular pivot the required spring constant had to be determined. Taking the minimum useful values determined for the drag force and the core displacement of the differential transformer a maximum allowable effective spring constant for the balance flexure system was calculated. First a ratio between the moment arms about the pivot point of the drag force and the transformer core was set. Since the floating wall surface element was to be restricted to small displacements it was felt that the transformer moment arm should be the longer of the two in order to get as large a movement as possible for the transformer core. The ratio was set at 3:2 for convenience. The effective spring constant of the flexure system is defined as

$$\frac{M}{\theta} = \frac{FR}{\theta} \quad , \tag{2}$$

where M = moment about center of rotation

θ = angular displacement

F = drag force

R = moment arm of drag force .

Setting the transformer core moment arm at three inches, the drag force moment arm at two inches, the drag force at 6×10^{-7} lb., (1 percent of the minimum expected drag force) and the transformer core displacement at 0.000023 inches, the spring constant was calculated to be 0.157 inch-pounds per radian. This is the maximum value for the spring constant that will provide the desired sensitivity and resolution.

A Bendix pivot having a spring constant of 0.102 inch-pounds per radian and capable of supporting 8.5 lb. in compression and 19.0 lb. in tension was chosen. This pivot is only 0.25 inches in diameter and 0.40 inches long and will allow angular rotations of ± 30°.

C. Null Force System

The last major component of the balance to be examined was the system

for providing a restoring moment to counteract the moment of the drag force and null the balance. Instead of using a variable strength electromagnet as did Smith and Walker a permanent magnet with a moveable conductor suspended in its field was chosen. It was felt that the permanent magnet would provide a more uniform and constant magnetic field. The variation in the restoring moment is obtained by varying the direct current through the moveable conductor which is one side of a wire coil that is fastened to the balance beam and extends into the gap between the magnet pole pieces. This can be done easily and quite accurately. The force created in this manner conforms to Ampere's Law in the form

$$F = BNIL \times 10^{-4} , \qquad (3)$$

where F = force in newtons

B = magnetic flux density in gauss

NI = product of number of conductors and current per conductor

L = length of conductors in meters .

A permanent magnet of Alnico V was taken from a discarded ammeter. New pole pieces of soft iron were machined and soldered to the Alnico V slug. The magnet was energized and then artificially aged by being subjected to moderate heat and vibration until it stabilized at a strength of 3100 gauss. The dimension across the face of the pole pieces was 0.67 inches (0.017 meters) and was taken to be the same as the effective conductor length L in the above equation. For this magnet to produce a force on a conductor equal to the maximum expected drag force, which was previously calculated as 1.2×10^{-4} lb. (5.4×10^{-4} newtons), the coil must have a total of 0.102 ampere turns. A coil wound with 10 turns then requires only 10.2 milliamps of current to counteract a drag force of 1.2×10^{-4} lb. Consequently the coil can be made small so as to fit into a narrow gap between the magnet pole pieces and batteries can be used to provide the current.

THE PROTOTYPE BALANCE

A. Design

After making the initial studies into the feasibility of a null-type skin friction balance it was felt that a prototype instrument would be advantageous for checking out all of the involved principles and components. The prototype balance was made as simple as possible while employing all of the operating features and important dimensions that would be used in the operational balance. The resulting instrument is shown in the sketch of Figure 2.

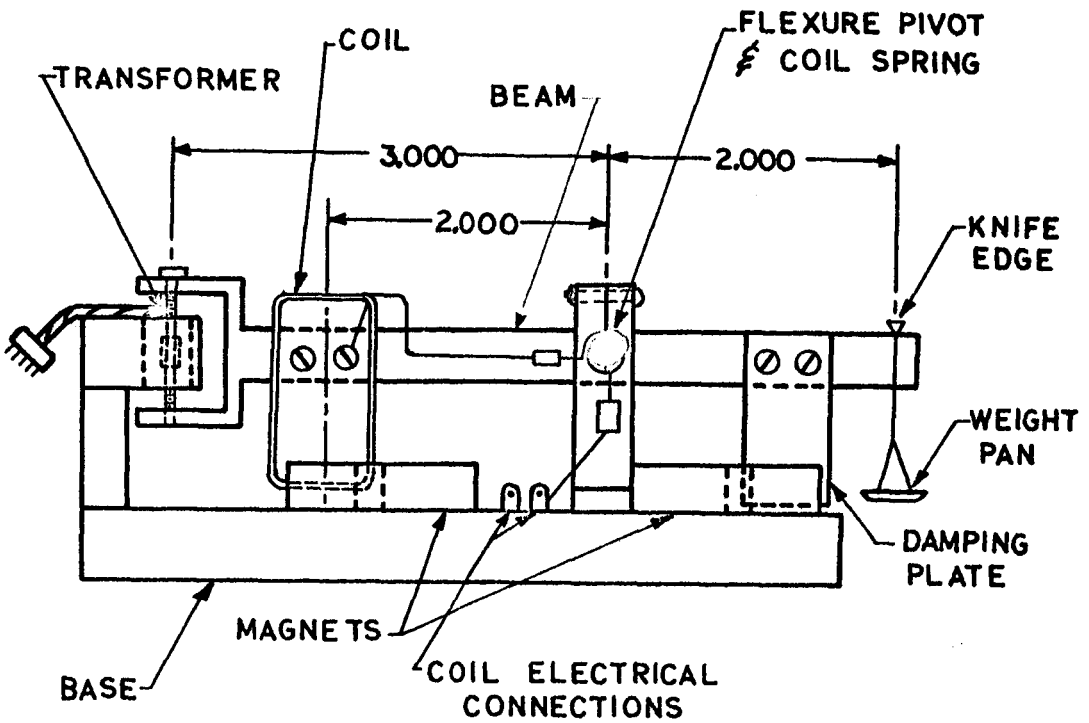

FIGURE 2. THE PROTOTYPE BALANCE

A simple beam was attached to a flexure pivot which was mounted in a fixed frame. A pan for holding calibration weights was hung on a knife edge at a point on one end of the beam 2.0 inches from the pivot axis. The core of a Schaevitz transformer was fixed to the other end of the beam at a distance 3.0 inches from the pivot axis. A coil wound with 10 turns of #28 magnet wire was fixed to the beam centered about a point 2.0 inches from the pivot axis and on the opposite side of the axis from the weight pan. The transformer case was fixed to the balance frame and centered so that the core could move within the cavity of the case but not touch it. The permanent magnet was also attached to the frame in a position so that the moving coil would be centered in the gap between the pole pieces. A second magnet was fixed to the frame and a copper plate that extended into the gap between the magnet poles was attached to the beam. This provided a system for damping beam oscillations.

The beam was statically balanced to give a zero moment at the flexure pivot for zero weight in the weight pan. One end of the moving coil was grounded to the beam which had electrical continuity through the flexure pivot to the balance frame. The other end of the coil was connected to a beryllium copper coil spring that was centered on the pivot axis and attached by means of an insulated mount to the frame. Direct current was supplied to the moving coil through the beryllium copper spring. The spring was one of the type used in sensitive ammeters. It added a negligible amount to the restoring moment of the flexure system but it allowed the electrical lead to be brought out from the beam without any flexing wires that would interfere with free movement of the beam.

B. Electrical System

The electrical instrumentation system developed for the prototype balance is also being used with the operational balance. Several problems were involved with the electrical system which will be explained in the following description. A schematic diagram of the complete electrical system is shown in Figure 3.

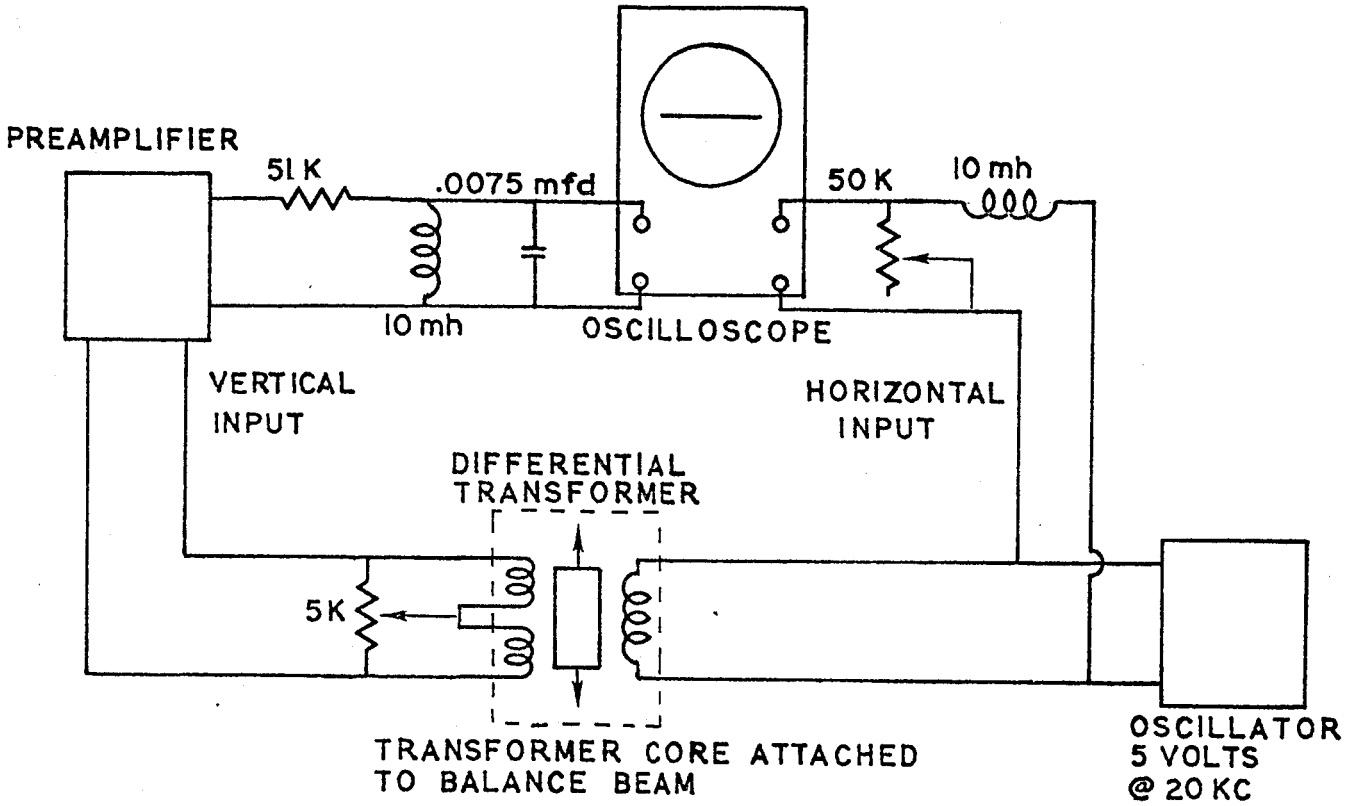

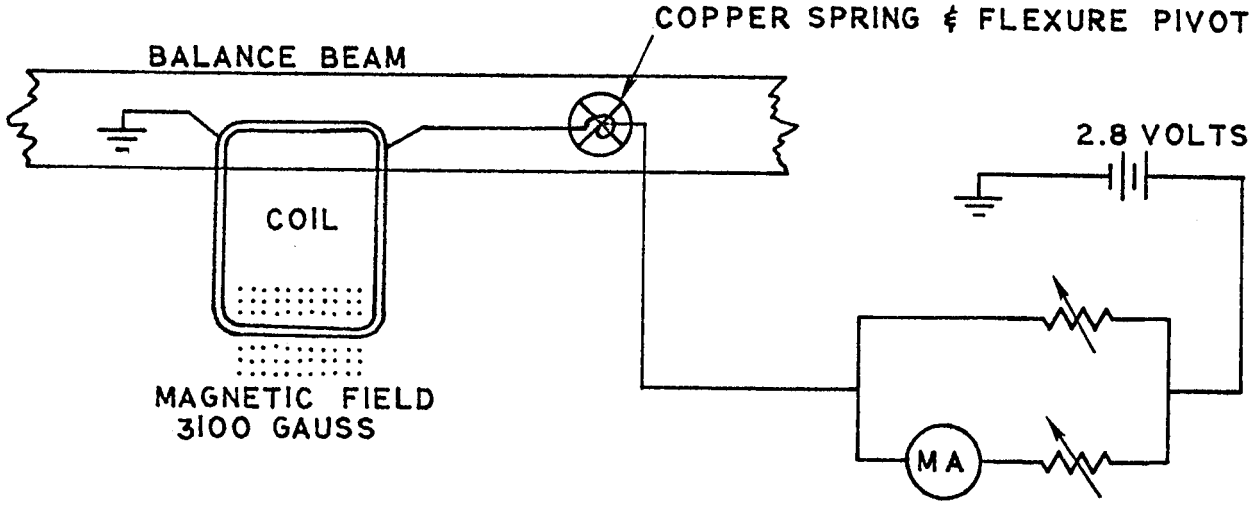

FIGURE 3. SCHEMATIC DIAGRAM OF THE
BALANCE ELECTRICAL SYSTEM

Direct current was supplied to the moving beam coil by mercury batteries having a voltage of 2.8 volts. The circuit was divided into two parallel branches. The current in one branch could be adjusted to overcome slight static unbalance and initially null the system, and the current in the second branch was used to cancel the applied forces. The currents in both branches were controlled by variable resistances in series with the batteries. The current in the second branch was variable from 62 microamps to 19 milliamps and could be read with an accuracy of 1% over the entire range.

The Schaevitz transformer was powered by an audio oscillator providing a 5 volt input with a frequency of 20 kilocycles per second. This type of transformer operates on the principle that a movement of the core relative to the windings causes a change in transformer reactance. The change in reactance causes a change in output voltage of the transformer which can easily and accurately be related to the core displacement. The transformer configuration and external circuitry are shown schematically in Figure 3. The two secondary coils are connected in opposition such that the output voltage is a linear function of the position of the iron core. A 5,000 ohm potentiometer is connected across the output to allow reduction of the voltage signal at the null position of the transformer core. A typical output signal curve is shown in Figure 4.

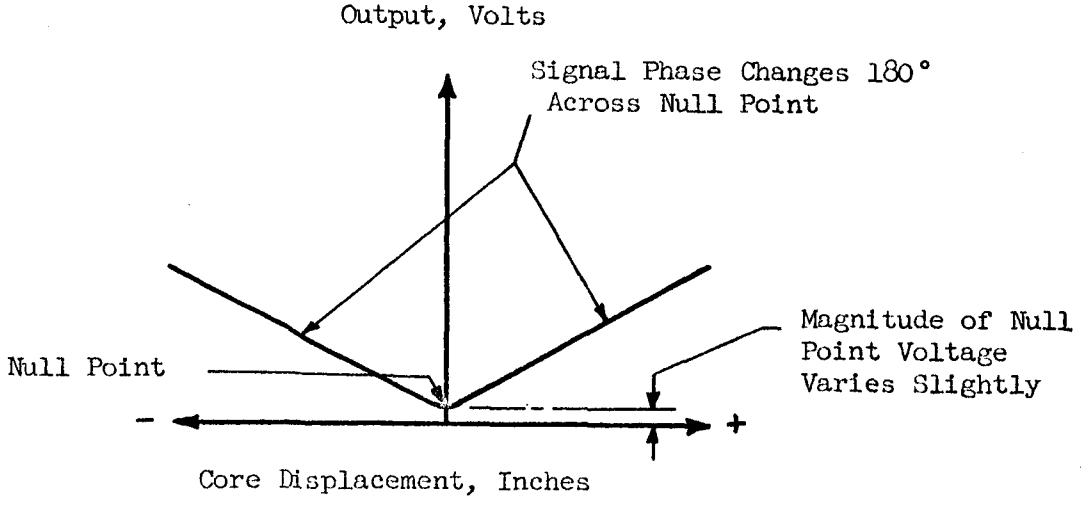

Figure 4. Transformer Output as a Function of Core Displacement

In order to sense small displacements of the transformer core, and hence small changes in output voltage, it was necessary to set the transformer core so that its null position corresponded with the null position of the balance. The null output signal was then adjusted to a minimum by means of the potentiometer across the transformer output. The exact value of null point voltage may vary as the signal from the oscillator varies in strength or frequency, but in any case the minimum value always occurs with the core in the same position. Thus, to null the balance, it is only necessary to adjust the current through the moving beam coil until a minimum output signal is obtained at the transformer.

There are several ways by which to monitor the transformer output signal. Since only the amplitude of the a-c signal is of interest in sensing a displacement of the core, an RMS voltmeter can be used with fair success provided it has adequate sensitivity. The a-c signal can also be rectified and read on a d-c volt meter, but in both of these cases the inherently slow response time of the meter causes problems in finding the null setting.

The method chosen for monitoring the transformer signal in this balance system proved to be faster and more reliable than either of those mentioned above. The a-c signal from the transformer output is fed into a pre-amplifier and then into the vertical input of an oscilloscope. The same signal from the oscillator (5 volts, 20 kc) that excites the transformer is fed into the horizontal input of the oscilloscope. The resulting oscilloscope trace is a closed loop. When the transformer, and hence the balance, is nulled the loop is collapsed flat, closed, and horizontal. When the transformer core moves away from the null position the loop rotates through an angle that is proportional to the core displacement. The system is rebalanced to the null condition by adjusting the current in the moving beam coil until the oscilloscope trace is again horizontal. The response time is the same as that of the balance system since the oscilloscope adds no additional damping. Also the direction of rotation of the scope trace indicates the side of the null position to which the transformer core has moved due to a 180° phase shift in the signal as the core passes through the null point.

A filter was found to be necessary in the vertical input signal due

to harmonic content in the transformer output. Without filtering, the harmonics, especially the third, in the 20 kc signal caused the oscilloscope trace to have a rippled appearance. A filter designed to reduce the third harmonic produced a satisfactorily smooth trace. A phase shifting circuit was added to the horizontal input to allow phase matching of the vertical and horizontal signals. This was necessary to keep the scope trace from opening into a loop as it rotates from the null position.

The prototype balance was calibrated over a force range of 0.18 milligrams (4×10^{-7} lbs.) to 53.7 milligrams (1.2×10^{-4} lbs.). The current through the secondary circuit leg of the moving beam coil was adjusted to achieve a nulled condition for the balance while the current in the primary circuit leg was initially maintained at a small value which was treated as a tare reading. Calibration weights cut from aluminum foil were used to load the balance. The calibration curve was exactly linear as expected. There was essentially no scatter in the data points except for the smallest forces, and this scatter was only of the same order as the uncertainty in the weighing of the smallest calibration weights. The calibration proved to be very repeatable with a calibration constant of 0.19 milliamps of current per milligram of force.

After calibration,the prototype balance was mounted on the framework of the boundary layer channel to check the response of the system to vibration. No significant effects of vibration were encountered as the channel was run through its operating range. This can be attributed to the fact that the natural frequency of the balance system was approximately one cycle per second while the vibrations in the boundary layer channel were on the order of 30 cycles per second and with very small amplitude.

THE SKIN FRICTION BALANCE

A. Construction

After the feasibility of the balance system was verified by the favorable results from the prototype model an operational skin friction balance was designed and fabricated. A photograph of the balance is shown in Figure 5. Noticeable components are the two magnets, the beam coil, the Schaevitz transformer, and some of the adjustment screws. The balance is shown mounted in a sub-section of the boundary layer channel. The operational balance is essentially the same as the prototype with respect to the major components and general arrangement, but some of the details require further description. Unless noted otherwise, all parts are made of aluminum.

1. Beam Assembly

The beam assembly consists of a rigid beam 5.40 inches in length with the core of a Schaevitz transformer attached near one end at a point 3.0 inches from the pivot axis and the floating wall surface element (hereafter referred to as a disk) attached to the other end so that the skin friction drag force acts at a distance of 2.0 inches from the pivot axis. The diameter of the disk is 1.250 inches and the surface area is 1.233 square inches. A 10-turn coil of #28 magnet wire is located with its center 2.0 inches from the pivot axis on the opposite side of the pivot from the disk. Electrical leads from the coil are identical to those on the prototype balance with one being grounded to the beam and the other brought out through a beryllium copper coil spring. A thin copper plate is attached to the beam near the disk to act in conjunction with a magnet on the frame as a damping system. The beam assembly is fastened to a flexure pivot with set screws.

2. Frame

The balance frame is a rigid assembly to which is attached the transformer case, the two magnets, and the beam assembly via the flexure pivot. The frame attaches to a base with adjustable screws that alternately push and pull between the frame and base allowing adjustments in height and tilt of the frame with respect to the base. The frame members that hold the flexure pivot and the transformer case are adjustable in all directions in

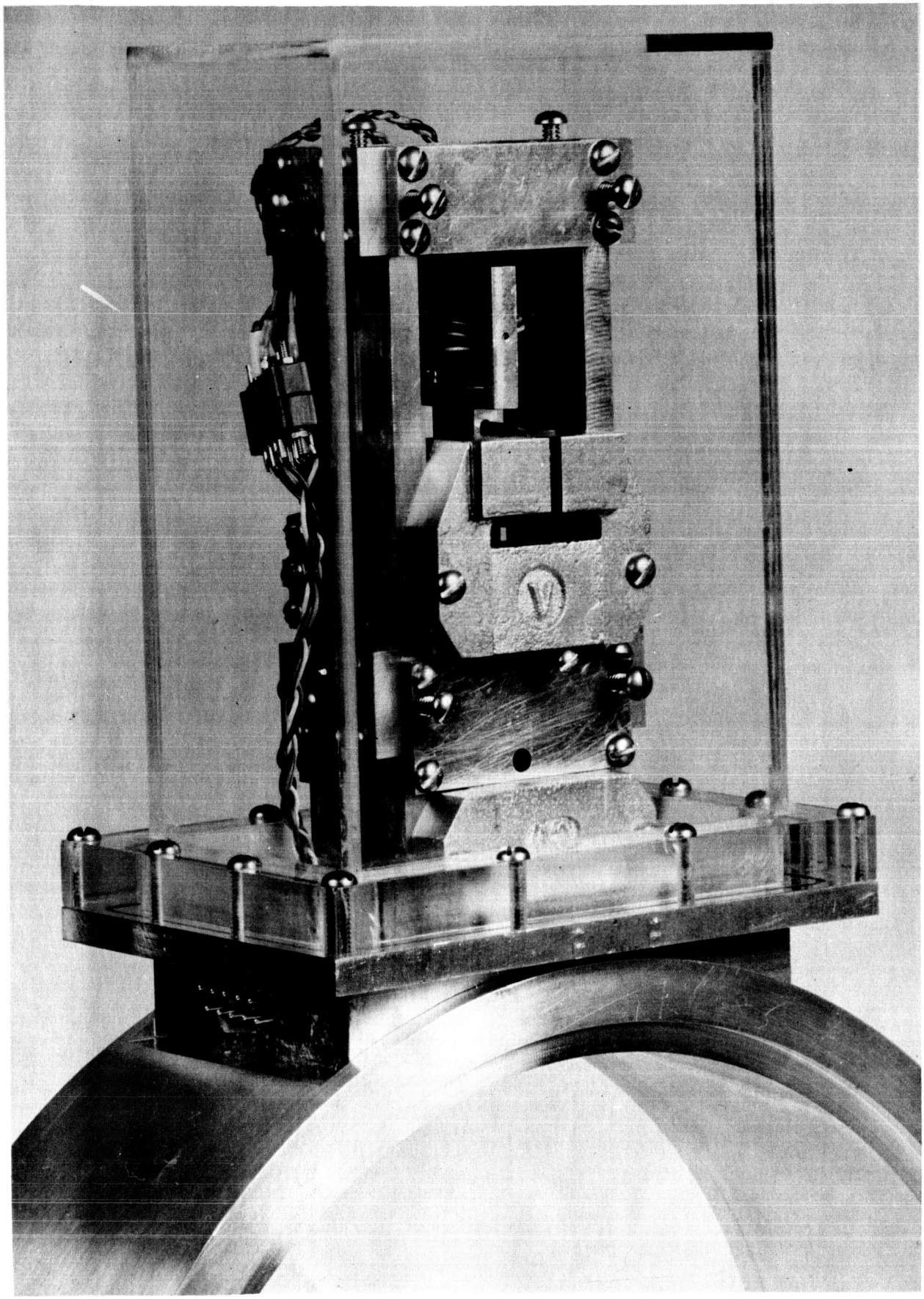

Figure 5. The Skin Friction Balance Shown Mounted in a Sub-section of the Boundary Layer Channel.

a horizontal plane, and the member holding the transformer case can also be adjusted in height and tilt with respect to the frame in the same manner as that in which the frame is adjusted with respect to the base. These various adjustments allow the disk to be aligned accurately in the base of the balance assembly and the transformer case to be positioned accurately with respect to the transformer core.

3. Base

The base of the balance system is a rectangular block to which the balance frame is attached. The base has a cylindrical extension 1.625 inches in diameter that passes through the wall of a section of the boundary layer channel. The end of this extension is machined to exactly match the curvature of the inside surface of the channel section. A 1.260-inch diameter hole through the cylindrical extension serves as the cavity for the balance disk providing a gap of 0.005 inches between the two. The resulting gap area is 1.7% of the disk area. According to Coles (reference 4) this size gap should not cause significant effects in the balance measurements when used in a flow with moderate pressure gradient.

4. Cover

A plexiglass cover protects the balance from dirt and dust, and it prevents convection air flows outside the boundary layer channel from acting on the beam and causing it to move. The cover also seals off the boundary layer channel from air leakage through the balance assembly.

The assembled balance was adjusted until the disk was centered in the base cavity and aligned with it. An 80 power stereoscopic microscope and a sensitive dial indicator were used to check the disk position. The disk was set with its surface recessed approximately 0.00003 inches inside the surrounding surface of the base. Previous investigators (references 4, 5, 6) have found that slightly recessed floating elements cause no significant errors in friction drag force measurements, while even the smallest extension of the element beyond the wall surface will introduce appreciable discrepancies due to the drag caused by the dynamic pressure of the flow acting on the exposed edge of the element. The ideal arrangement would be to have the element exactly flush with the wall, but due to practical limitations in locating the element it is safer to set it slightly recessed.

B. Calibration

A horizontal bar for holding calibration weights was attached to the balance beam. The axis of the bar passes through the pivot axis of the balance. Weights can be hung at either end of the bar on pins placed 1.200 inches from the pivot axis. Weights can be hung on one pin to simulate a specific drag force and on the other pin to cancel a specific drag force. This second feature allows forces too large for direct measurement with the balance to still be measured by canceling a known and sufficient portion of the force with a known weight. The remainder of the unknown force can then be measured conventionally with the balance. Access to the calibration bar is through openings on either side of the cover. The openings are sealed with plugs while readings are taken. Neither the calibration bar nor the cover openings are known in Figure 5 as they were added after the photograph was made.

The balance was calibrated while it was mounted in the boundary layer channel. It should be mentioned here that a special section of tubing was fabricated for the channel for use with the skin friction balance. The special section is actually a set of 9 sub-sections ranging from 0.50 to 23.38 inches in length which allow the balance position to be varied along the length of the section in increments of 0.50 inches. The balance is mounted in a 2.88-inch sub-section.

To prepare the balance for calibration, adjustable weights were set to statically balance the beam assembly so that it would be near the null position. The electrical system from the prototype model was connected to the balance and the final null adjustments were made with the direct current in the beam coil.

Because of the difference in the moment arm lengths of the calibration bar and the balance beam a ratio of 0.6 exists between calibration forces and actual drag forces. Calibration weights from 17.7 to 72.8 milligrams were used covering a drag range from 10.6 to 43.7 milligrams (2.3×10^{-5} to 9.6×10^{-5} lbs.). The calibration curve is shown in Figure 6 with the data points plotted as effective drag forces.

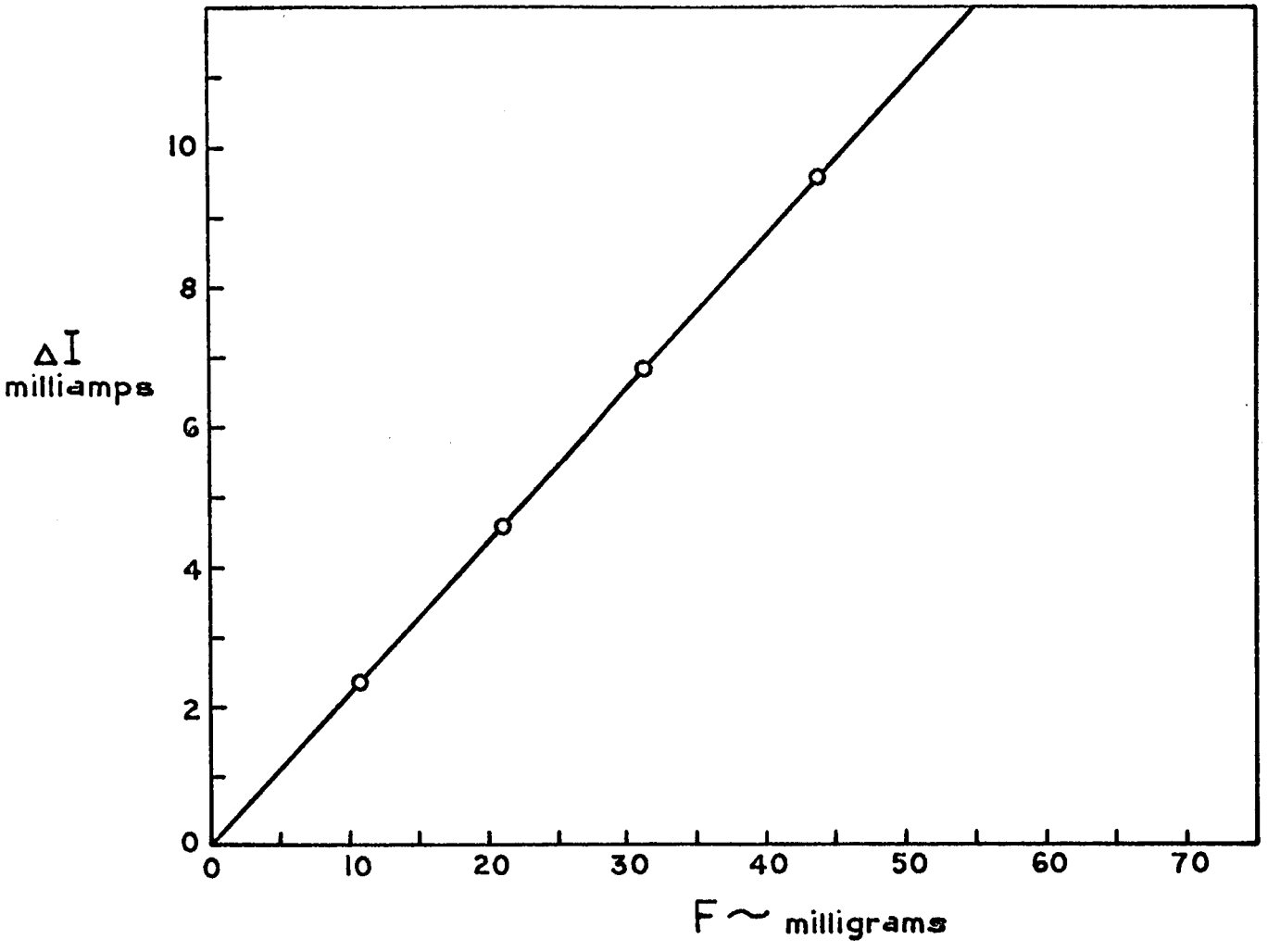

FIGURE 6. SKIN FRICTION BALANCE STATIC CALIBRATION

C. Skin Friction Measurements

The first tests of the skin friction balance were made in a laminar boundary layer. Since the skin friction drag for laminar flows on a flat plate can be accurately calculated from theory this was believed to be a good method for checking the performance of the balance. The magnitude of the skin friction drag for the laminar boundary layer is much smaller than for a turbulent boundary layer and thus creates an even more rigorous test for the balance than would the turbulent boundary layer.

The skin friction balance was placed at several locations in the boundary layer channel, and measurements were made over a range of Reynolds numbers based on distance from the effective beginning of boundary layer growth. The measured forces ranged from 1.3×10^{-6} lb to 8.5×10^{-6} lb. The skin friction drag measurements were reduced to skin friction coefficients and plotted versus Reynolds number. The data are shown in Figure 7a. As can be seen the agreement with theory (reference 10) is very good with the largest discrepancies being about 1 percent except at the highest Reynolds numbers which are approaching the region of transition from laminar to turbulent flow. These tests satisfactorily verified the accuracy of the balance in measuring a known friction drag force.

The next step in testing the balance was the measurement of local skin friction in a turbulent boundary layer. Skin friction coefficients were determined from drag measurements made at five values of the Reynolds number based on the momentum thickness of the boundary layer as determined from velocity profiles measured with a total head probe. The data are shown in Figure 7b. To explain the manner in which the data are presented a brief review of the development of the correlation used is in order.

The data were initially compared to the two-dimensional relation, (reference 6),

$$\frac{1}{\sqrt{C_f}} = 4.13 \log Re_\theta + 2.90 \qquad (4)$$

All of the skin friction coefficients were smaller than those predicted by

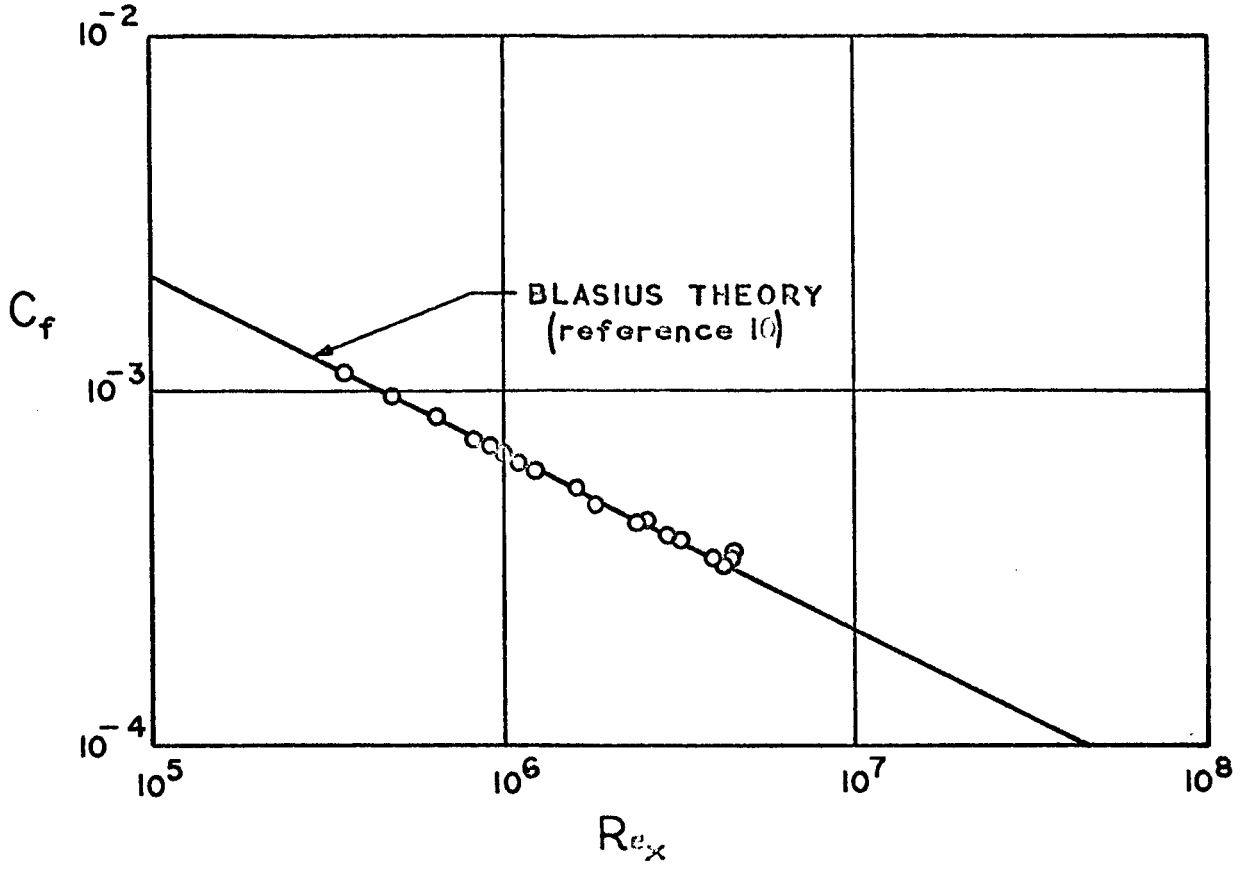

FIGURE 7(a). LAMINAR SKIN FRICTION COEFFICIENTS

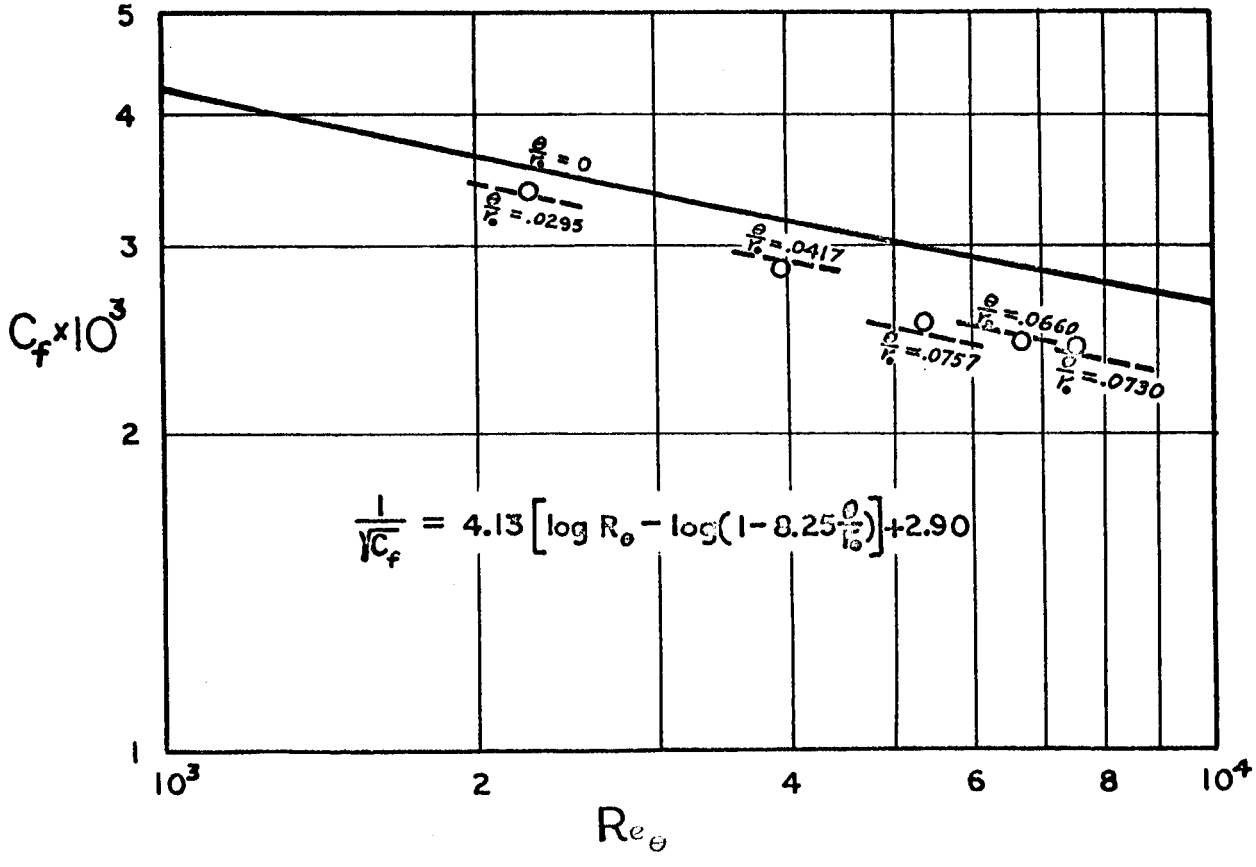

FIGURE 7(b). TURBULENT SKIN FRICTION COEFFICIENTS

the two-dimensional relation at the same Reynolds number. The data were also compared to friction factor measurements in fully developed pipe flow and were again found to be smaller. Taking this into consideration, along with the fact that turbulent boundary layer flow in the channel actually corresponds to turbulent entrance flow in a pipe due to the thickness of the boundary layer compared to the radius of the channel, it was concluded that the boundary layer was three-dimensional in nature and any attempt to correlate the skin friction data would have to take three-dimensional effects into account. Realizing the significance of this situation with respect to the future turbulent boundary layer experiments it was decided at this point to re-derive the C_f, Re_θ relation for an axisymmetric three-dimensional boundary layer.

To begin, the velocity profiles were compared with the universal law of the wall to assure that the boundary layer was in equilibrium. The law of the wall is expressed as

$$\phi = A \ln \eta + B, \tag{5}$$

where

$$\phi = \frac{u}{u_\tau}, \quad \eta = \frac{\rho y u_\tau}{\mu}, \quad u_\tau = \sqrt{\frac{\tau_o}{\rho}},$$

and A and B are constants. The law of the wall states that in the portion of a turbulent boundary layer near the wall the velocity distribution is dependent only upon the density and viscosity of the fluid and the shear stress at the wall. This implies that the flow near the wall is uninfluenced by flow conditions at a greater distance, in particular by the free-stream velocity and pressure gradient. Thus the law of the wall is applicable in three-dimensional as well as two-dimensional flow.

The measured velocity profiles for the largest and smallest Reynolds numbers of the data are shown in Figure 8 compared to both the theoretical expression for the law of the wall and Coles' (reference 4) expression obtained from measurements in the boundary layer on a flat plate. As can be seen the data satisfactorily conform to the law of the wall. The agreement of the data with the well proven relation in these plots is another indication of the accuracy of the skin friction balance due to the fact that measured values of

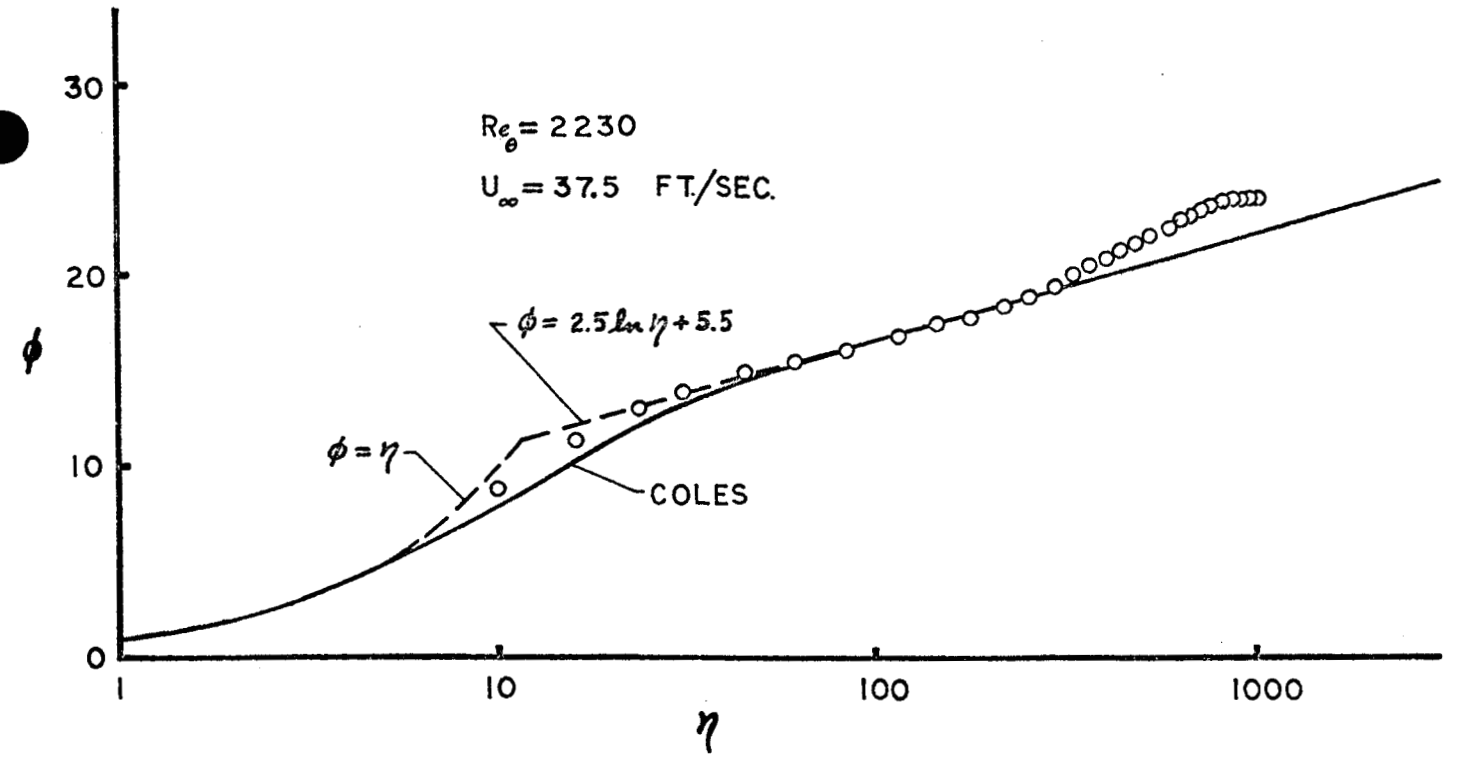

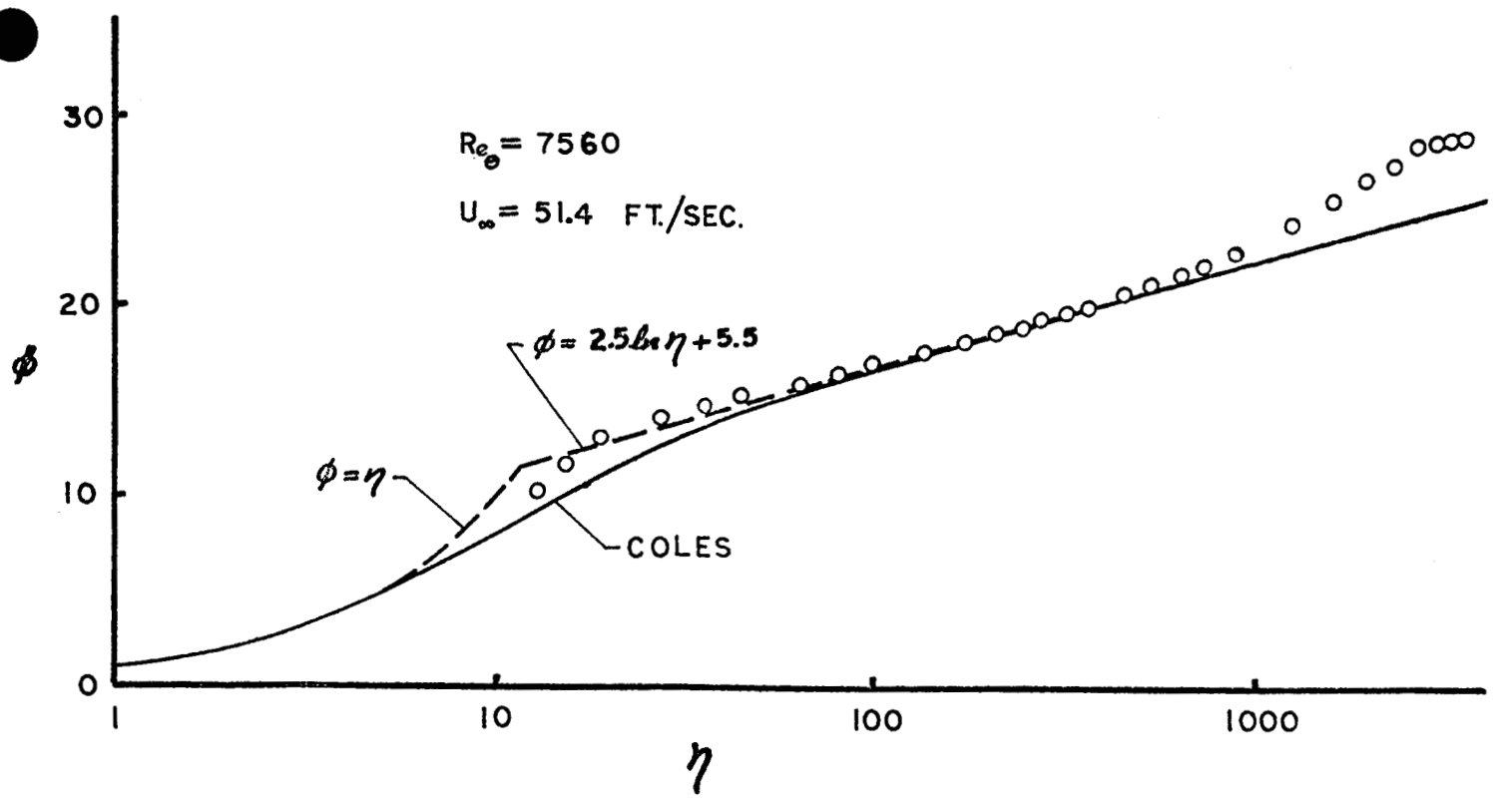

FIGURE 8. LAW OF THE WALL VELOCITY PROFILES

shear stress appear in both the ϕ and η coordinates.

The momentum thickness for axisymmetric flow inside a tube of radius r_o can be expressed as the quadratic

$$r_o \theta - \tfrac{1}{2}\theta^2 = \int_o^{r_o} \frac{u}{U_\infty}\left(1 - \frac{u}{U_\infty}\right) r\, dr \quad . \tag{6}$$

With measured velocity profile data, equation (6) can be graphically integrated and solved for θ.

Equation (6) is re-written with the velocity profile now expressed in the form of the law of the wall. Making the substitution $\phi/\phi_\infty = u/U_\infty$ and dividing both sides of the equation for θ by r_o^2 one obtains the non-dimensional expression

$$\frac{\theta}{r_o} - \tfrac{1}{2}\left(\frac{\theta}{r_o}\right)^2 = \int_1^o \frac{\phi}{\phi_\infty}\left(1 - \frac{\phi}{\phi_\infty}\right) \frac{r}{r_o} \frac{d\left(\frac{r}{r_o}\right)}{d\left(\frac{\phi}{\phi_\infty}\right)} d\left(\frac{\phi}{\phi_\infty}\right). \tag{7}$$

Noting that r is defined as positive outward from the tube centerline and y is defined as positive inward from the tube wall, the substitution

$$\frac{r}{r_o} = 1 - \frac{y}{r_o} = 1 - \frac{\mu}{\rho u_\tau}\frac{\eta}{r_o}$$

can be made. Also the derivative

$$\frac{d\left(\frac{r}{r_o}\right)}{d\left(\frac{\phi}{\phi_\infty}\right)}$$

can be written as

$$\frac{d\left(\frac{r}{r_o}\right)}{d\left(\frac{\phi}{\phi_\infty}\right)} = -\frac{d\left(\frac{y}{r_o}\right)}{d\left(\frac{\phi}{\phi_\infty}\right)} = -\frac{\mu}{\rho u_\tau r_o}\frac{d\eta}{d\left(\frac{\phi}{\phi_\infty}\right)} \quad . \tag{8}$$

Solving for η from equation (5), differentiating with respect to $\frac{\phi}{\phi_\infty}$, and substituting in equation (8) gives

$$\frac{d\left(\frac{r}{r_o}\right)}{d\left(\frac{\phi}{\phi_\infty}\right)} = -\frac{\mu}{\rho u_\tau r_o}\frac{\phi_\infty}{A}\exp\left[\left(\frac{\phi}{\phi_\infty}\right)\frac{\phi_\infty}{A} - \frac{B}{A}\right] . \qquad (9)$$

Making this substitution in equation (7), reversing the limits of integration, and changing the sign leaves the integral equation

$$\frac{r_o \rho u_\tau}{\mu}\left[\frac{\theta}{r_o} - \tfrac{1}{2}\left(\frac{\theta}{r_o}\right)^2\right]$$

$$= \int_o^1 \frac{\phi}{\phi_\infty}\left(1 - \frac{\phi}{\phi_\infty}\right)\left(1 - \frac{\mu}{r_o \rho u_\tau}\eta\right)\frac{\phi_\infty}{A}\exp\left[\left(\frac{\phi}{\phi_\infty}\right)\frac{\phi_\infty}{A} - \frac{B}{A}\right] d\left(\frac{\phi}{\phi_\infty}\right) . \qquad (10)$$

This equation can be integrated in closed form. Performing an order of magnitude analysis and dropping the smallest terms from both sides of the equation in a manner consistent with the derivation of the two-dimensional relation of C_f the resulting expression is

$$Re_\theta = A \exp\left[\frac{\phi_\infty}{A} - \frac{B}{A}\right] - \frac{A\mu}{4\rho u_\tau r_o}\exp\left[2\left(\frac{\phi_\infty}{A} - \frac{B}{A}\right)\right] . \qquad (11)$$

As r_o in equation (11) approaches infinity the second term on the right side approaches zero and the expression reduces to the two-dimensional relation. Thus the equation is equivalent to the two-dimensional expression plus a correction term which disappears as three-dimensional effects become insignificant.

To reduce the equation to the final form in terms of C_f and Re_θ an approximation is made. The two-dimensional form of equation (11) is

$$Re_\theta = A \exp\left[\frac{\phi_\infty}{A} - \frac{B}{A}\right] . \qquad (12)$$

Substituting equation (12) in the second term of equation (11) gives

$$Re_\theta = A \exp\left[\frac{\phi_\infty}{A} - \frac{B}{A}\right] - \frac{Re_\theta \mu}{4 \rho u_\tau r_o} \exp\left[\frac{\phi_\infty}{A} - \frac{B}{A}\right] \quad . \qquad (13)$$

This approximation in the correction term is considered justified in light of the previous simplifications of the equation. Rearranging equation (13), taking the logarithm of both sides, and making the substitution $\phi_\infty = \sqrt{\frac{2}{C_f}}$ gives

$$\frac{1}{\sqrt{C_f}} = \frac{A}{\sqrt{2}} \ln Re_\theta - \frac{A}{\sqrt{2}} \ln\left[1 - \frac{\phi_\infty}{4A}\left(\frac{\theta}{r_o}\right)\right] - \frac{A}{\sqrt{2}} \ln A + \frac{B}{\sqrt{2}} \quad . \qquad (14)$$

Converting from natural to common logarithms and taking the constants in the two-dimensional portion of equation (14) as those determined in reference 6 the final relation becomes

$$\frac{1}{\sqrt{C_f}} = 4.13 \log Re_\theta + 2.90 - 4.13 \log\left[1 - \frac{\phi_\infty}{4A}\left(\frac{\theta}{r_o}\right)\right] \quad . \qquad (15)$$

It will be noticed that ϕ_∞ appears in the correction term of equation (15). Consequently, this equation does not give an explicit expression for C_f since ϕ_∞ is equal to $\sqrt{2/C_f}$. It is known that the variation in ϕ_∞ is small over the range of Re_θ of interest here, therefore taking this into consideration along with the approximations made in deriving the final equation, it was believed reasonable to simplify the correction term by approximating the coefficient of θ/r_o as a constant. Treating all of the data points as equally valid the constant coefficient of θ/r_o was then adjusted to give the best fit to the data. The value of the constant was determined to be 8.25, giving agreement between the measured data and the derived theory within ± 2.5%. It may be possible to achieve better average agreement by readjusting the constant after more data is obtained.

An attempt was made to compare the data of Nikuradse (reference 11) for fully developed turbulent pipe flow with the three-dimensional axisymmetric expression for C_f and Re_θ given in equation (15). It was hoped that these data would lend further credence to the analysis;i.e., would show fully developed pipe flow to be a limiting case for the general analysis. However, it was found

that the constant in the correction term in equation (15) had to be much smaller to correlate Nikuradse's data. Inspection of the analysis proved this to be reasonable due to the fact that fully developed turbulent pipe flow and turbulent pipe entrance flow differ significantly in their agreement with the universal law of the wall velocity profile at its outer edge. Since this theoretical profile is integrated over limits of ϕ from zero to measured values of ϕ_∞ it means that the value of η, which is a measure of the shear layer thickness, is considerably different for the two types of flow when the integration is carried to the same measured value of ϕ_∞. In practice, this situation is handled by adjusting the constants to fit experimental data. Furthermore, the concept of a momentum thickness loses its significance for fully developed turbulent pipe flow since, from the momentum equation, the skin friction for this case is shown to be exactly balanced by the longitudinal pressure gradient. For these reasons it was concluded that the analysis derived herein, in its present state, is not applicable to fully developed pipe flow.

Additional experimental evaluation of the analysis presented will be accomplished during the planned investigations. This analysis will be of significance in evaluating the effects of the disturbance producing elements on the turbulent boundary layer characteristics.

At this point it was felt that concrete proof of the accuracy of the skin friction balance in turbulent flow had still not been established although it was implied by the data of Figures 7 and 8. An attempt was made to achieve fully developed flow in the boundary layer channel by operating at the lowest practical velocity and surveying the flow at the largest practical x distance. Due to operating limitations of the facility there was very little latitude in the Reynolds number based on pipe diameter. This form of the Reynolds number is defined as

$$Re_D = \frac{\bar{u}\, D}{\nu}$$

where, $\bar{u}$ is average or bulk velocity based on the mass flow rate

D is pipe diameter

ν is kinematic viscosity of the fluid

The measured velocity profile showed that the flow was not quite fully developed but was very close. Also, measurements of the static pressure in the vicinity of the measuring station showed the pressure gradient to be constant. An analysis by Deissler (reference 12) predicts that the velocity profile near the wall, and hence the skin friction, stabilizes more rapidly than the outer portion of the profile in developing pipe flow. Hence, the relation of C_f to Re_D for fully developed flow should be applicable when the flow is almost fully developed.

The average velocity of the flow in the boundary layer channel was obtained by integrating the measured profile, and Re_D and C_f were calculated based on this velocity and the measured skin friction. The values were $Re_D = 35,250$ and $C_f = 0.00568$. Using Nikuradse's (reference 11) correlation for fully developed turbulent flow in smooth pipes a value of $C_f = 0.00566$ was calculated for the same Reynolds number. The percent disagreement between the measured C_f and that predicted by Nikuradse is 0.35%. It is felt that this result along with those mentioned previously satisfactorily verifies the accuracy of the skin friction balance.

SUMMARY

In summarizing, the skin friction balance has been shown to be a very sensitive instrument and has provided consistent and repeatable data. The sensitivity is almost unlimited depending only on the extent to which the user wishes to go in amplifying and measuring the output signal. The repeatability has been shown to be better than one percent both in the calibration and in shear stress measurements. The skin friction balance is now in use as a permanent component in the boundary layer channel instrumentation complex.

ACKNOWLEDGEMENTS

This work has been done in the LTV Research Center Aerophysics Group under the supervision of Dr. John Harkness. Many helpful ideas were offered by various members of this group. In particular the author wishes to express his appreciation to Mr. W. A. Meyer for initially suggesting this type of balance and for his assistance with the electrical instrumentation, and to Mr. C. H. Parker for his valuable skill in fabricating and assembling the skin friction balance. The construction of this instrument, as well as the program in which it is being used, is supported by independent research and development funds of Ling-Temco-Vought, Inc. and by the National Aeronautics and Space Administration under Contract No. NASw-730.

REFERENCES

1. Wells, C. S. Jr., and Spangler, J. G., "A Facility for Basic Boundary Layer Experiments", LTV Research Center Report No. 0-71000/2R-32, November 1962.

2. Kempf, G., "Neue Ergebnisse der Widerstandsforschung", Werft, Reedereie, Hafen, Vol. 10, No. 11, 1929, pp. 247-253.

3. Schultz-Grunow, F., "New Frictional Resistance Law for Smooth Plates", NASA TM 986, September 1941.

4. Coles, D., "Measurements in the Boundary Layer on a Smooth Flat Plate in Supersonic Flow", Ph.D thesis, California Institute of Technology, 1953.

5. Dhawan, S., "Direct Measurements of Skin Friction", NACA TR 1121, 1953.

6. Fenter, F. W., "Analysis and Direct Measurement of the Skin Friction of Uniformly Rough Surfaces at Supersonic Speeds", Presented at the National Summer Meeting, Institute of the Aeronautical Sciences, Preprint No. 837, Los Angeles, California, July 1958.

7. Bidwell, J. M., "Application of the von Kármán Momentum Theorem to Turbulent Boundary Layers", NACA TN 2571, December 1951.

8. Smith, D. W., and Walker, J. H., "Skin Friction Measurements in Incompressible Flow", NASA TR R-26, 1959.

9. Eastman, F. S., "Flexure Pivots to Replace Knife Edges and Ball Bearings", Engineering Experiment Station, University of Washington, Bulletin No. 86, November, 1935.

10. Schlichting, H., Boundary Layer Theory, McGraw-Hill, New York (1955), p. 108.

11. Nikuradse, J., "Gesetzmässigkeiten der turbulenten Strömung in glatten Rohren", VDI-Forschungsheft 356, 1932.

12. Deissler, R. G., "Analysis of Turbulent Heat Transfer and Flow in the Entrance Regions of Smooth Passages", NACA TN 3016, 1953.